Supporting Information for "Glacial runoff buffers drought through the 21st century—but models disagree on the details"

L. Ultee[1], S. Coats[2]

[1]Department of Earth, Atmospheric, and Planetary Sciences, Massachusetts Institute of Technology

[2]Department of Earth Sciences, University of Hawaii at Manoa

Contents of this file

1. Text S1 to S3

2. Captions to multi-panel figures S2 and S3

3. Figures S1 to S5

Introduction

All analysis shown in the main text is reproducible and extensible for any of the 56 basins using the Jupyter notebook and code we have provided on GitHub (see link in Acknowledgements). We encourage readers interested in detailed results for a specific basin to make use of the material provided there. The public code also allows users

———

Corresponding author: L. Ultee, Department of Earth, Atmospheric, and Planetary Sciences, Massachusetts Institute of Technology, Cambridge, MA 02139 USA. (ehultee@umich.edu)

July 9, 2020, 2:52pm

to change time scales of analysis—for example, presenting running means over 5-year rather than 30-year windows, or calculating SPEI at a 27-month rather than 15-month timescale—and examine SPEI under the RCP 8.5 rather than RCP 4.5 emissions scenario.

For readers' convenience, we include below extended results for each of the 56 basins we analyzed, for the same time scales and climate scenario shown in the main text. The results are presented as multi-page sets of panels that replicate the panels shown in Figures 2 and 3 of the main text, but with all 56 basins rather than the 4 examples shown in the text. Figure S2 shows the glacial effect on mean SPEI. Figure S3 shows the glacial effect on SPEI variance. The panels in both figures were computed with climate scenario RCP 4.5, examining SPEI with a 15-month integration timescale, comparing statistics with a 30-year running window.

Text S1. SPEI computation

SPEI is computed by aggregating and normalizing a simple climatic water balance,

$$D_i = P_i - PET_i, \tag{S.1}$$

where P_i is the precipitation in time step i, PET_i is the potential evapotranspiration in the same time step, and D_i is their difference. We take precipitation P_i directly from the output of each GCM that we analyze, aggregated to basin scale as described in main text section 2. We estimate PET_i with the Penman-Montieth method, following Allen, Pereira, Raes, and Smith (1998). To calculate PET requires surface temperature, surface pressure, surface specific humidity, and surface net radiation from the GCM. Surface wind is set to be constant, as PET has been shown to be insensitive to the inclusion of surface

wind from GCMs (Cook et al., 2014). All methods for calculating PET directly follow those in Cook et al. (2014).

Text S1.1. Sensitivity to integration timescale

SPEI includes a user-selected timescale of integration, which can be adjusted to study different types of drought and different parts of the hydroclimate system. Short timescales relate to availability of water as soil moisture and headwater river discharge, while longer timescales relate to reservoir storage, downstream water discharge, and changes in groundwater storage (Vicente-Serrano et al., 2009). In our analysis, we present SPEI computed with a relatively long integration timescale of 15 months. This choice reflects our focus on hydrological drought in semi-arid mountain basins dependent on frozen precipitation and seasonal snowmelt (see main text section 2 and McEvoy et al., 2012). We also computed SPEI at a range of integration timescales to ensure our results for the 15-month timescale were not anomalous. One example is below; results for all basins and timescales are available on our public repository.

Figure S1 shows the glacial effect on mean SPEI in the Tarim basin (compare with Figure 2b), with SPEI computed at seven different timescales of integration. The qualitative patterns of the glacial effect on SPEI are similar across integration timescales: some models show ΔSPEI increasing nearly monotonically, while others show an initial increase with a peak near midcentury and subsequent decline. Inter-GCM differences in ΔSPEI are broadly consistent across timescales, though the ordering of GCMs from smallest glacial effect in a basin to largest does vary. The magnitude of the glacial effect ranges from 0.1 SPEI units to 2 SPEI units at different timescales. Although the smallest-magnitude

effect appears at the shortest timescale of integration in the Tarim basin, there is no monotonic relationship between ΔSPEI magnitude and integration timescale. That is, the magnitude of the effect we analyse does not scale linearly with the SPEI timescale.

Text S1.2. Uncertainties in non-glacial components of SPEI

One of the strengths of SPEI for analysing drought under a future changed climate is that it accounts for changing atmospheric demand for moisture. This accounting is not possible with drought metrics that account solely for precipitation, such as the Standardized Precipitation Index (McKee et al., 1993; World Meteorological Organization & Global Water Partnership, 2016). However, the methods used to compute atmospheric demand for moisture, in the form of PET, are a source of uncertainty in SPEI and other PET-based drought metrics. For example, Milly and Dunne (2016) found that the Penman-Montieth method for computing PET overpredicts non-water-stressed evapotranspiration under future climate change. Yang, Roderick, Zhang, McVicar, and Donohue (2019) suggest a method to correct PET under future climate change by including a varying stomatal conductance term in the Penman-Montieth calculation.

We have focused here on the large glacial contribution to SPEI, and uncertainties in the non-glacial components are not central to our analysis. Nevertheless, to ensure our results were robust, we recomputed all SPEI timeseries following the corrected PET method of Yang et al. (2019). We then compared SPEI_N and the glacial effect $\text{SPEI}_W-\text{SPEI}_N$ (see Methods) for each basin computed with and without the correction. Figure S4 shows per-basin differences in each, normalized by the single-basin multi-model mean of each value to facilitate comparison across basins. We find that although the Yang et al. (2019) correction

can make a large difference in $SPEI_N$ for individual basins, with a maximum of 107%

difference for a single basin (Figure S4a), in most cases the correction is inconsequential.

The percent difference in the glacial effect, $SPEI_W - SPEI_N$, is an order of magnitude lower

(Figure S4b). A mean of -0.07% difference and an absolute maximum of 0.6% difference

in glacial effect due to the inclusion of the Yang et al. (2019) correction confirm that our

use of the uncorrected Penman-Montieth method does not impact our analysis or results.

Text S2. Accounting for glacial runoff

We account for glacial runoff in each basin during the period 1980-2100 using the runoff

simulations of Huss and Hock (2018). Their model is forced by monthly near-surface

air temperature and precipitation from global climate reanalysis (Dee et al., 2011) and

CMIP5 GCM projections (Taylor et al., 2011), downscaled to each individual glacier. The

initial area of each glacier is defined as the "glacier catchment" for the duration of the

simulation. That is, the portion of a basin within a glacier catchment does not change

over time, even as the area of the glacier itself does change. Runoff is simulated at the

individual glacier level and includes all water exiting the catchment, both melted snow

and ice as well as rain falling within the catchment boundary. These monthly glacier

runoff totals are then aggregated to the basin scale.

In the Huss and Hock (2018) glacial model output, some portion of the GCM-derived

precipitation falling within a basin is also counted within the basin glacial runoff. To

avoid double-counting precipitation in our $SPEI_G$ moisture source term, we scale GCM-

derived precipitation by each basin's unglaciated area (Equation 1) and add it to glacial

runoff scaled by the basin's glaciated area. PET is then subtracted from this sum, which

is equivalent to assuming that both precipitation falling in the unglaciated part of the basin and glacial runoff from the glaciated part of the basin are encountering atmospheric demand for moisture.

Text S3. Quantifying ensemble mean and range

In the present study, we have focused on identifying and interpreting qualitative differences among GCM-projected SPEI with and without glacial runoff. This approach makes evident, for example, that no one GCM is consistently wetter or drier than another across basins, and that differences in both land and atmosphere schemes shape projected SPEI in glaciated basins (see main text).

Future studies of hydrological drought in glaciated basins may wish to quantify inter-basin differences in the glacial effect. To that end, we have supplied code in our public repository to compute the inter-GCM mean and interquartile range of SPEI for each basin, emissions scenario, and inclusion/exclusion of glacial runoff—the so-called structural uncertainty in the glacial effect.

Figure S5 plots these ensemble statistics for the Tarim Basin, both with and without glacial runoff (compare with main text Figure 1). The ensemble mean and interquartile range further reinforce the findings of the main text: without glacial runoff, the Tarim basin would be drying throughout the century, while with glacial runoff conditions are projected to be wetter in the 21st century than the 20th.

Figure S2. Glacial effect on 30-year running mean SPEI by basin, for all 56 large-scale glaciated basins worldwide, under emissions scenario RCP 4.5. Figures are styled in the same way as main text Figure 2: Curves shown are a 30-year running mean of

the difference SPEI_W- SPEI_N, where "W" and "N" denote "with glacial runoff" and "no accounting for glaciers", respectively. A different vertical scale has been applied to each plot to aid readability. Grey shading indicates the period when 30-year running means include years for which the glacier model has not yet been switched on.

Figure S3. Glacial effect on 30-year running SPEI variance by basin, for all 56 large-scale glaciated basins worldwide, under emissions scenario RCP 4.5. Figures are styled in the same way as main text Figure 3: Curves shown are the difference of running 30-year variances, $\text{Var}(\text{SPEI}_W)$-$\text{Var}(\text{SPEI}_N)$, where "W" and "N" denote "with glacial runoff" and "no accounting for glaciers", respectively. A different vertical scale has been applied to each plot to aid readability. Grey shading indicates the period when 30-year running statistics include years for which the glacier model has not yet been switched on.

References

Allen, R. G., Pereira, L. S., Raes, D., & Smith, M. (1998). Crop evapotranspiration—guidelines for computing crop water requirements. In *FAO Irrigation and drainage paper* (Vol. 56). United Nations Food and Agriculture Organization.

Cook, B. I., Smerdon, J. E., Seager, R., & Coats, S. (2014). Global warming and 21st century drying. *Climate Dynamics*, *43*(9-10), 2607–2627. doi: 10.1007/s00382-014-2075-y

Dee, D. P., Uppala, S. M., Simmons, A. J., Berrisford, P., Poli, P., Kobayashi, S., . . . Vitart, F. (2011). The ERA-Interim reanalysis: configuration and performance of the data assimilation system. *Quarterly Journal of the Royal Meteorological Society*, *137*(656), 553–597. doi: 10.1002/qj.828

Huss, M., & Hock, R. (2018). Global-scale hydrological response to future glacier mass loss. *Nature Climate Change*, *8*(2), 135–140. doi: 10.1038/s41558-017-0049-x

McEvoy, D. J., Huntington, J. L., Abatzoglou, J. T., & Edwards, L. M. (2012). An evaluation of multiscalar drought indices in Nevada and Eastern California. *Earth Interactions*, *16*(18), 1–18.

McKee, T. B., Doesken, N. J., & Kleist, J. (1993). The relationship of drought frequency and duration to time scales. In *Proceedings of the 8th Conference on Applied Climatology, 17-22 January 1993, Anaheim, CA.* Boston, MA.

Milly, P. C., & Dunne, K. A. (2016). Potential evapotranspiration and continental drying. *Nature Climate Change*, *6*(10), 946. doi: 10.1038/nclimate3046

Taylor, K. E., Stouffer, R. J., & Meehl, G. A. (2011). An overview of CMIP5 and the experiment design. *Bulletin of the American Meteorological Society*, *93*(4), 485–498. doi: 10.1175/BAMS-D-11-00094.1

Vicente-Serrano, S. M., Beguería, S., & López-Moreno, J. I. (2009). A multiscalar drought index sensitive to global warming: The standardized precipitation evapotranspiration index. *Journal of Climate*, *23*(7), 1696–1718. doi: 10.1175/2009JCLI2909.1

World Meteorological Organization, & Global Water Partnership. (2016). *Handbook of drought indicators and indices* (Tech. Rep.). Geneva, Switzerland: Integrated Drought Management Programme (IDMP).

Yang, Y., Roderick, M. L., Zhang, S., McVicar, T. R., & Donohue, R. J. (2019). Hydrologic implications of vegetation response to elevated CO_2 in climate projections. *Nature Climate Change*, *9*(1), 44. doi: 10.1038/s41558-018-0361-0
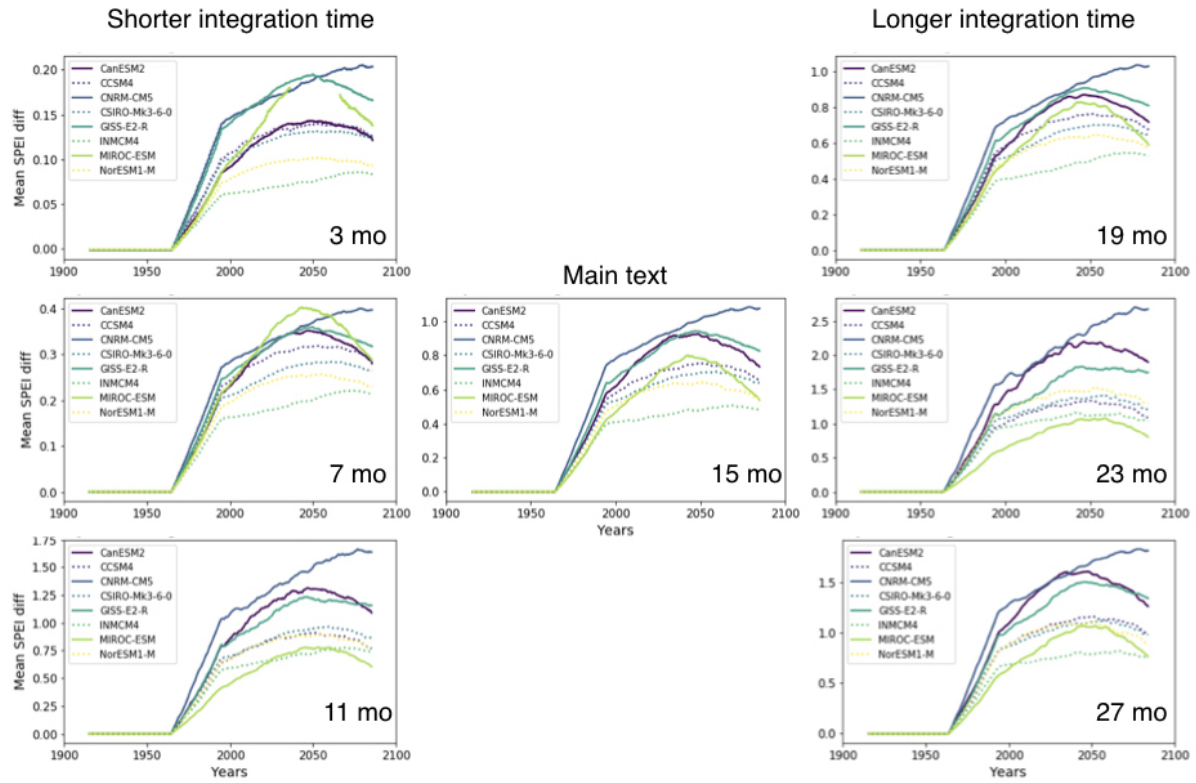
Figure S1.   Comparison of glacial effect on SPEI over the 21st century when SPEI is computed with integration timescales ranging from 3 to 27 months. The central panel shows the 15-month integration timescale analysed in the main text of this work; shorter integration timescales appear to the left and longer timescales to the right. Note different y-axis scales in different panels.
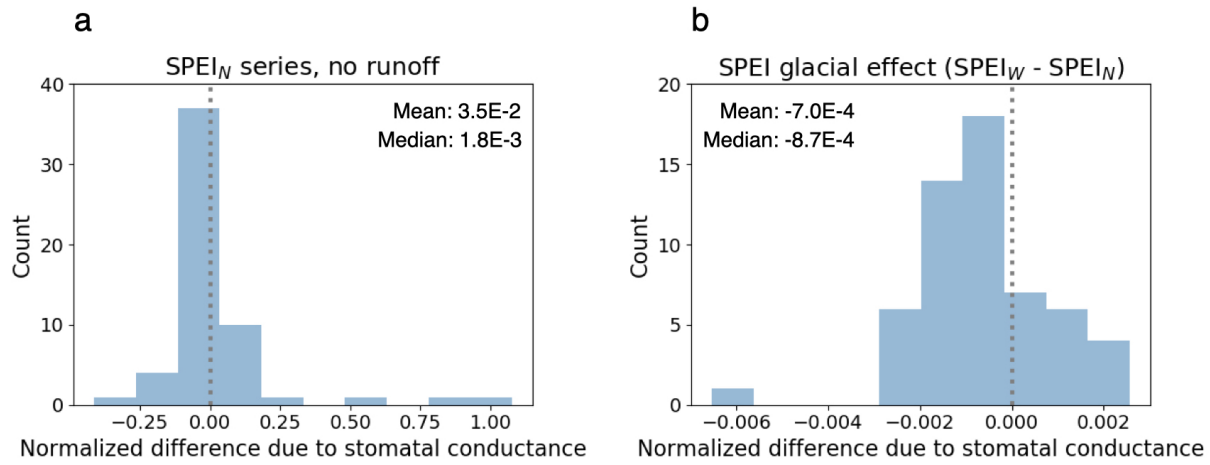
a

SPEI$_N$ series, no runoff

Mean: 3.5E-2
Median: 1.8E-3

Normalized difference due to stomatal conductance

b

SPEI glacial effect (SPEI$_W$ - SPEI$_N$)

Mean: -7.0E-4
Median: -8.7E-4

Normalized difference due to stomatal conductance

Figure S4.   Histograms of pairwise percent difference after accounting for variable stomatal conductance in (a) SPEI$_N$, the SPEI timeseries for each basin computed with no glacial runoff, and (b) SPEI$_W$−SPEI$_N$, the glacial effect on SPEI timeseries for each basin.
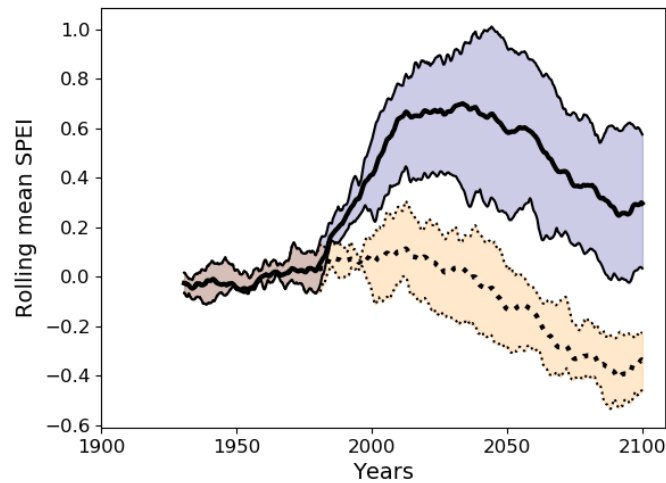
Figure S5.   Multi-GCM ensemble mean and interquartile range of SPEI for the Tarim basin, with (solid, blue fill) and without (dashed, orange fill) glacial runoff.

July 9, 2020, 2:52pm